CORE
Metadata, citation and similar papers at core.ac.uk
Provided by Elsevier - Publisher Connector

Available online at www.sciencedirect.com
ScienceDirect
Biochimica et Biophysica Acta 1778 (2008) 214–228
Biochimica et Biophysica Acta
BBA
www.elsevier.com/locate/bbamem

Local and translational dynamics in DNA–lipid assemblies monitored by solid-state and diffusion NMR

Cecília Leal [a,*], Dick Sandström [b,1], Pernilla Nevsten [c], Daniel Topgaard [a,*]

[a] *Physical Chemistry 1, Lund University, POB 124, SE-221 00 Lund, Sweden*
[b] *Physical Chemistry, Arrhenius Laboratory, Stockholm University, SE-106 91 Stockholm, Sweden*
[c] *Materials Chemistry, Lund University, POB 124, SE-221 00 Lund, Sweden*

Received 17 April 2007; received in revised form 2 September 2007; accepted 24 September 2007
Available online 10 October 2007

Abstract

The influence of electrostatic interactions on the dynamic properties of complexes containing DNA and mixtures of cationic- (DDA) and zwitterionic (DLPC) lipids are studied by means of NMR. The systems are arranged in lamellar membrane stacks intercalated by DNA molecules. This is confirmed by ^{31}P-NMR, where a superposition of an axially symmetric powder pattern arising from the phospholipid membrane and an asymmetric tensor due to DNA can be fitted to the experimentally observed lineshape. The local mobility and order is assessed using two solid-state NMR techniques applicable to samples with natural isotopic abundance: WIdeline SEparation (WISE) and Separated Local Field (SLF) spectroscopy. Both experiments yield highly resolved ^{13}C spectra in the direct dimension. The indirect dimension contains information about molecular dynamics through the ^{1}H dipolar linewidth (WISE) or the ^{1}H–^{13}C dipolar coupling constant (SLF). The experiments suggest that DNA is static while it induces an increased disorder in the hydrocarbon chains as compared to the parent lipid case. DDA chain order is more affected than DLPC due to the attractive electrostatic interaction between DNA and the cationic lipid. Translational dynamics of the lipids and the water was measured with the Pulsed Field Gradient STimulated Echo (PFG STE) technique. The influence of lamellar domain size and the angular dependence of the diffusion coefficients and nuclear relaxation times on the results of the PFG STE experiments are discussed. The local water diffusion coefficient is reduced by a factor four from the value of bulk water, and increases as the DLPC content is increased. We observe two lipid components with an order of magnitude difference in diffusion coefficients in the DNA:DDA:DLPC precipitate and these are assigned to DLPC (fast) and DDA (slow). Cationic lipid (DDA) diffusion is decreasing a factor of 2 when DLPC is added to the pure DNA:DDA system, indicating DNA-induced lipid segregation within the bilayer and the transition from locally 2D to 1D diffusion of the DDA. The results show that DNA–lipid electrostatic interactions reduce the long-range lipid mobility but locally enhance the hydrocarbon chain dynamics by perturbing the preferred lipid packing.
© 2007 Elsevier B.V. All rights reserved.

Keywords: DNA-lipid assemblies; Membrane local mobility; Membrane local order; Lateral diffusion; Domain size; Domain formation; Solid-state NMR; Diffusion NMR

1. Introduction

The building block of cell membranes is a self-assembled lipid bilayer that is involved in regulating the dynamic events in and out of cells and cell constituents. DNA has a number of contacts with membranes *in vivo*. Enveloped viral DNA is one example where lipid bilayers beneath the protein capsid are in close contact with DNA [1]. Another case is DNA replication where the idea of DNA being anchored to a specific site in the cell membrane, where various enzymes and initiators proteins could be captured and where segregation of newly synthesized chromosomes could occur [2], still represents a good replication model. Inspired by this, DNA–membrane complexes have been isolated yielding successful *in vitro* replication [3]. The virus case motivated the design of lipids that are able to envelope large amounts of DNA without undesirable immune responses, as potential tools for gene delivery [4,5]. In all *in vivo* and *in*

* Corresponding authors. Currently at: Materials Department, University of California Santa Barbara, California 93106, USA.
E-mail addresses: cecilial@mrl.ucsb.edu (C. Leal), Daniel.Topgaard@fkem1.lu.se (D. Topgaard).
[1] Currently at: Bruker BioSpin Scandinavia AB, Polygonvägen 79, SE-187 66 Täby, Sweden.

0005-2736/$ - see front matter © 2007 Elsevier B.V. All rights reserved.
doi:10.1016/j.bbamem.2007.09.035

vitro membrane complexes, the structure and dynamic properties of the lipid molecules in the bilayer play very important roles. The membrane protein world is extremely vast and this work relates only to membranes and DNA, nevertheless from a lipid perspective there are similarities as both DNA and proteins are biopolymers in close contact with a lipid matrix. In fact, studying solely lipid behavior can unravel important information related to the entity interacting with the lipid membrane (DNA, proteins, drugs, and others). Interestingly, in some cases it has been demonstrated that some lipid hydrocarbon chains are almost straight (all-*trans*) but others need to be considerably disordered in order to be able to wrap around the bulky side chains of the protein [6]. In the virus case, the properties of the membrane are crucial during infection; in bacteriophage PRD1 thousands of lipid components are asymmetrically distributed between membrane leaflets displaying a surprising degree of conformational order [1]. In artificial gene-carriers, lipid membrane charge density and "fluidity" within the DNA–lipid complex [7,8] have been directly related to transfection efficiency. While structural studies are abundant, the dynamics of DNA–lipid complexes are less explored. Recently, Natali and co workers [9] investigated lipid dynamics in the ns-time scale with neutron scattering techniques and it was observed that out-of-plane lipid motions are favored for DNA–lipid complexes at the isolectric point. Conformational order of lipids within DNA–lipid aggregates has been investigated by fluorescence [7] where membrane "fluidity" was correlated with efficiency of DNA transfection. Infrared studies [10] suggest that there is an increase in conformational disorder of lipid hydrocarbon tails upon DNA interaction.

In this work, we use solid-state and diffusion NMR to investigate the local molecular order as well as local and translational dynamics of concentrated lamellar complexes, schematically represented in Fig. 1a, containing DNA and a mixture of two lipids: cationic didodecyl dimethylammonium (DDA) and zwitterionic dilauroyl-*sn*-glycero phosphocholine (DLPC). The objective is to determine the molecular mobility of the three components in the system, particularly, if the electrostatic attraction between DNA and the cationic DDA induces DDA/DLPC demixing in the membrane. NMR is a

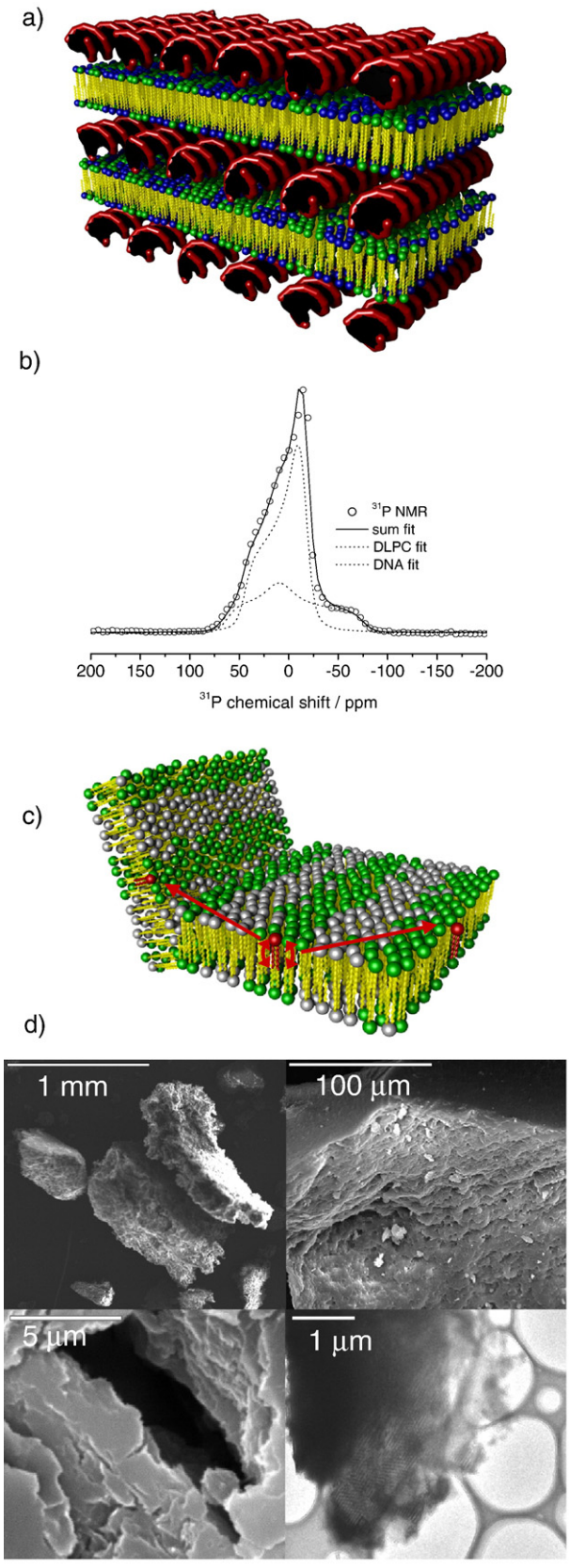

Fig. 1. (a) Schematic representation of the supramolecular arrangement in stoichiometric DNA–lipid complexes first suggested by Rädler et al. [24]. The bilayers composed of a mixture of cationic lipid (DDA) and zwitterionic phospholipid (DLPC) are intercalated by DNA molecules forming a lamellar structure. The zwitterionic and the cationic lipids comprising the bilayer are expected to locally demix with the cationic (green spheres) lipids more concentrated around DNA. (b) Static ^{31}P spectrum of fully hydrated DNA:DDA:DLPC (1:1:1). As indicated in the figure legend: the dotted data is the experimental ^{31}P spectrum, the dashed lines are the deconvoluted components originating from the phospholipid DLPC and the DNA, and the solid line represent the sum of the components. The spectrum is a superposition of an axially symmetric CSA tensor typically obtained for lamellar phases and an axially asymmetric tensor for DNA. (c) Illustration of "local" and "translational" mobility of the lipid molecule (marked in red) within the lipid bilayer and between lipid bilayer domains. (d) SEM and TEM images of DNA–DDA complex precipitates at different scales. The three SEM images show that the grain size varies from mm to µm; at higher magnification we can observe the layered morphology with flakes a few µm thick; the TEM image shows a precipitate flake displaying Moiré patterns indicating the overlap of ordered, randomly oriented, domains. (For interpretation of the references to colour in this figure legend, the reader is referred to the web version of this article.)

non-invasive method that can provide unique mobility and structural information at the molecular level. Other techniques, like for example fluorescence, can be useful to give information on lipid conformational order but require implementation of specific probes which can perturb the system. In addition, the probes classify as polar or apolar so the information associated with different lipids in a mixture is difficult to unravel.

With solid-state NMR techniques not only conformational order but also dynamics can be measured. In addition, different molecules and molecular sites can be resolved from high-resolution ^{13}C spectra. The ^{13}C chemical shift can be correlated with molecular mobility in the indirect dimension of two-dimensional (2D) experiments. These experiments are based on the fact that nuclear dipole–dipole interactions depend on the distance between the nuclei, the orientation of the dipolar interaction tensor relatively to the main magnetic field, and the motion of the molecule. For the WIdeline SEparation (WISE) experiment [11], the indirect dimension yields the ^{1}H dipolar linewidth, which can be related to the general "mobility" of the environment in which the studied molecular moiety resides. Here, the linewidth is estimated from the decay of the time domain signal. Separated Local Field spectroscopy (SLF) [12,13] gives values of the $^{1}H–^{13}C$ dipolar coupling, from which the order parameter of the corresponding C–H bond can be calculated. The local mobility information obtained by solid-state techniques is compared with the dynamics of the system on larger time and length scales by measuring the water and lipid diffusion coefficients using diffusion NMR [14].

2. Materials and methods

2.1. Materials

Calf thymus Na–DNA was purchased from Sigma and used as received. DNA concentration (in terms of base) was determined by UV using the molar extinction coefficient ε_{260}=6600 L mol^{-1} cm^{-1} at 260 nm [15]. The protein contamination indicator, A_{260}/A_{280}, was found to be 1.8 suggesting that the DNA solution was protein-free [15]. Sodium bromide (Riedel-deHaen extra pure quality) was used as received. The cationic lipid didodecyl dimethylammonium bromide, DDAB (Tokyo Kasei Kogyo Co., Ltd, >98% pure) and the zwitterionic lipid dilauroyl-*sn*-glycero phosphocholine, DLPC (Larodan Fine Chemicals, Malmö, Sweden, >98% pure) were used as received. The water used was from a Milli-Q filtration system (Millipore). D_2O was obtained from Dr. Glaser AG, Basel.

2.2. Sample preparation

The DNA–lipid complexes were prepared as described in [16]. In short, DDAB and DLPC powders were dissolved in chloroform in the required amounts. The solvent was evaporated in a vacuum oven at 30 °C for 2 days. The lipid film was then rehydrated and mixed with a Na–DNA solution (2 mM in 5 mM NaBr, pH=7.2) [17] under stirring. The concentration of Na–DNA in terms of charge was matching the DDAB concentration (2 mM). The white precipitate, formed within a minute after the addition of the lipid solution to the DNA solution, was equilibrated in solution for 24 h. It was then separated from the aqueous phase by filtration and washed extensively with water. The DNA–lipid precipitate was further dried in vacuum for 3 days. Three lipid mixtures were used: one containing only DDAB; a second containing DDAB and DLPC at 1:0.5 (mol:mol) ratio; and a third mixture DDAB:DLPC at 1:1 (mol:mol) ratio. The resulting precipitate DNA:DDA:DLPC should be electroneutral with essentially all Na and Br ions removed from Na–DNA and DDAB, respectively. Na and Br contents were below the detection limit of the optical emission spectrometry chemical analysis of the precipitate. The correctness of the lipid ratio was checked by integrating the areas in single pulse ^{13}C spectra.

For the solid-state NMR experiments, ~60 mg of dry DNA–lipid precipitate was loaded into a 4 mm, thin wall zirconia rotor (Varian Inc.) while being exposed to air with approximately 40% relative humidity. After spun overnight, the precipitate was fully hydrated by injecting a drop of water in the rotor containing the dry sample. The saturated samples were equilibrated overnight at room temperature before the actual measurements. Negligible water loss during the measurements was confirmed by weighing the rotors before and after the experiments.

For ^{31}P-NMR and the lipid diffusion experiments, dry DNA–lipid precipitate was put into a 5-mm NMR tube and excess D_2O was added. For the H_2O diffusion measurement, the precipitate was equilibrated 5 days at 99.5% relative humidity before being transferred to the NMR tube.

Scanning electron microscopy (SEM) was performed on gold coated DNA–lipid precipitate, attached to copper stubs with carbon tabs, using a JEOL JSM840A instrument, working at 20 kV accelerating voltage. Transmission electron microscopy (TEM) was performed on DNA–lipid precipitate placed on lacey carbon filmed copper grids using a Philips CM120 BioTWIN Cryoinstrument at 120 kV.

2.3. NMR

2.3.1. ^{31}P-NMR

Static ^{31}P-NMR spectra with 100 kHz spectral width were acquired at 81 MHz ^{31}P resonance frequency (4.7 T) on a Bruker DMX-200 spectrometer using a Bruker broadband probe. 16384 scans were accumulated using 14 μs 90° pulses, 4.5 μs receiver dead time, 1 s recycle delay, and 8 kHz ^{1}H decoupling during acquisition. The temperature was controlled with a Bruker VT unit to 25.0±0.1 °C.

2.3.2. Solid-state NMR

Magic Angle Spinning (MAS) experiments were carried out at 25±2 °C and 5 kHz spinning speed on a Chemagnetics Infinity-400 spectrometer (9.4 T) using a 4 mm triple-resonance MAS probe. ^{1}H MAS spectra were recorded using a spectral width of 15 kHz. High-resolution ^{13}C MAS spectra with a spectral width of 25 kHz were obtained and correlated with ^{1}H linewidth measurements using the WISE pulse sequence [11] shown in Fig. 2a. During ^{13}C signal detection, 20 kHz ^{1}H dipolar decoupling was applied with the two-pulse phase-modulated (TPPM) method [18]. Cross-polarization (CP) from ^{1}H to ^{13}C was performed during 4 ms for all the samples. As explained in a previous publication [19], samples comprised of species with a large difference in molecular mobility are preferably studied using a non-linear sampling of the indirect ^{1}H dimension in the WISE experiment. The direct ^{13}C dimension was evaluated with a standard Fourier transform while the ^{1}H dimension was evaluated by fitting an exponential, for the fast decaying components, or an exponentially damped cosine function, for the slowly decaying ones, to each peak in the series of 16 ^{13}C spectra.

Heteronuclear $^{1}H–^{13}C$ dipolar couplings were measured by the R-PDLF pulse sequence shown in Fig. 2b. This 2D experiment was recently introduced by Dvinskikh et al. [13] and incorporates R-type recoupling [20] into the proton-detected local field (PDLF) protocol [21]. The ^{1}H to ^{13}C polarization transfer (PT) was in this study carried out using CP (contact time=1.0 ms). The ^{1}H field strengths during dipolar recoupling and heteronuclear decoupling were 45 and 30 kHz, respectively. Further details of the R-PDLF scheme can be found elsewhere [13,22].

2.3.3. Diffusion

Pulsed Field Gradient Stimulated Echo (PFG STE) experiments (see Fig. 2c) were performed at 25.0±0.1 °C on a Bruker DMX-200 spectrometer with a Bruker DIF-25 gradient probe. For studies of lipid diffusion, the strengths G of δ=1.5 ms gradient pulses were linearly incremented in 128 steps to the maximal value of 9.6 T/m. An effective diffusion time $\Delta-\delta/3$ of 101.7 ms results from τ_1=2.6 ms and τ_2=100 ms. For water diffusion measurements, both τ_1 and τ_2

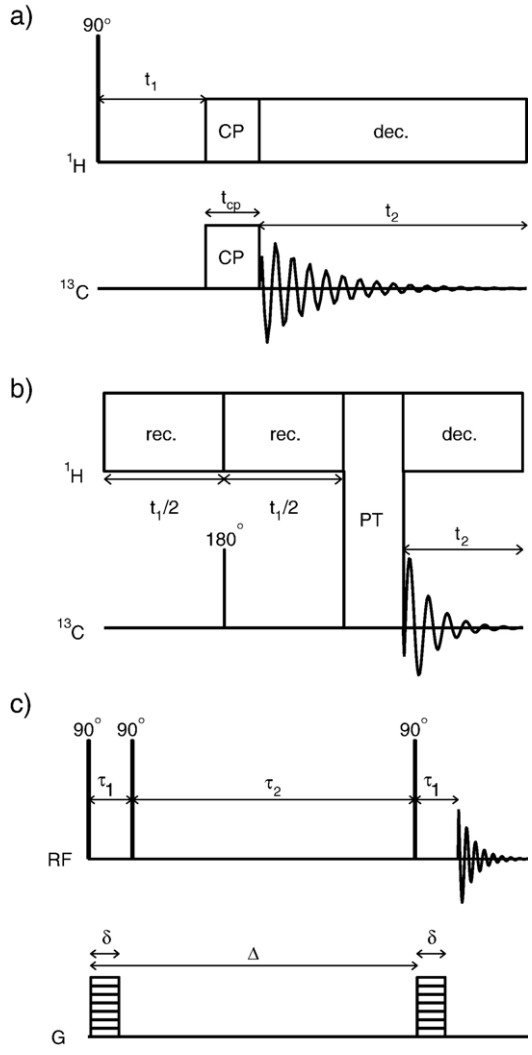

Fig. 2. (a) Pulse sequence for the MAS ^{1}H–^{13}C 2D WISE experiment: ^{1}H evolution during t_1 after a 90° pulse, followed by ^{1}H–^{13}C CP during t_{cp}, and ^{13}C detection with ^{1}H decoupling (dec) during t_2. (b) Pulse sequence for the MAS ^{1}H–^{13}C 2D R-PDLF experiment: ^{1}H–^{13}C dipolar recoupling (rec) during a variable ^{1}H evolution period t_1 (a ^{13}C 180° pulse is inserted at $t_1/2$ to suppress recoupled ^{1}H chemical shift anisotropy interactions), followed by ^{1}H to ^{13}C polarization transfer (PT), and ^{13}C signal observation during the detection period of t_2 with ^{1}H decoupling (dec). (c) Pulse sequence for the PFG STE experiment: a stimulated spin-echo is produced at time $2\tau_1+\tau_2$ by three 90° pulses. A pair of gradient pulses with amplitude G and duration δ encodes the signal for molecular displacements. The effective diffusion time is $\Delta-\delta/3$, where Δ is the time between the onset of the gradient pulses.

were set to 10 ms in order to attenuate the signal from the lipids on account of their rather short T_2. δ=0.5 ms gradient pulses were linearly incremented in 32 steps to 9.6 T/m using $\Delta-\delta/3$=20.5 ms.

3. Results and discussion

In this work, we explore the molecular order and dynamics in concentrated aggregates of DNA and lipids. The aggregates were prepared by adding to Na–DNA a charge matching lipid mixture composed of a double chain cationic lipid (DDAB) and a zwitterionic lipid (DLPC) at concentrations that lead to an associative phase separation. Essentially all the counterions are expelled to the aqueous phase and an isolectric DNA:DDA:DLPC complex is obtained [23]. The supramolecular structure [24,25] typically obtained for the resulting precipitate is schematically represented in Fig. 1a. It consists of a stack of lipid bilayers with DNA intercalated in-between described by two characteristic distances: repeat distance of the lamellar stack (d_{lam}) and distance between DNA molecules (d_{DNA}). The repeat distance of the unit cell and the in-plane distance between DNA molecules depend on lipid composition; an increasing fraction of the neutral lipid induces the lamellar stack to swell in the lateral direction and the DNAs to move further apart [24]. We observe these characteristics for our samples as well; d_{lam} and d_{DNA} for the lamellar DNA:DDA:DLPC complex with lipid composition (mol_{DDA}:mol_{DLPC}) 1:0, 1:0.5, 1:1 and 1:2 were obtained by Small Angle X-ray Scattering (SAXS). From lower DLPC content to higher d_{lam}/d_{DNA} (Å) are: 46.2/27, 50.7/31.4, 55.8/35.3 and 63/42.

3.1. ^{31}P-NMR

Both phospholipids and DNA exhibit characteristic ^{31}P chemical shift anisotropy (CSA) powder patterns and here we used this fact to verify the SAXS results and prove that the phospholids are indeed located in a bilayer structure. The CSA is described in terms of the 3×3 chemical shift tensor that relates the orientations of the molecular frame to the magnetic field. A full chemical shift tensor in principal axes can be decomposed into its isotropic and anisotropic parts and the isotropic chemical shift (δ_{iso}) corresponding to the average over all orientations can be related to the principal values δ_{xx}, δ_{yy}, and δ_{zz} as:

$$\delta_{iso} = \frac{1}{3}\left(\delta_{xx} + \delta_{yy} + \delta_{zz}\right) \quad (1)$$

The *anisotropy* (δ_{aniso}) and the *asymmetry* (η) parameters of the chemical shift tensor are defined as:

$$\delta_{aniso} = \delta_{zz} - \delta_{iso}, \quad (2)$$

$$\eta = \frac{\delta_{yy} - \delta_{xx}}{\delta_{yy} - \delta_{iso}}. \quad (3)$$

The principal values can be described according to many conventions, here we use:

$$|\delta_{zz} - \delta_{iso}| \geq |\delta_{xx} - \delta_{iso}| \geq |\delta_{yy} - \delta_{iso}| \quad (4)$$

According to this definition, rapid axial rotation of the phospholipid around the bilayer normal in a lamellar phase results in η=0. The resulting ^{31}P-NMR lineshape is a powder like spectrum with a high field peak and a low field shoulder for chemical shift orientations perpendicular and parallel to the magnetic field, respectively [26]. For a sample of solid DNA the tensor lacks axial symmetry and η is typically around 0.5, giving rise to a broad ^{31}P spectrum with a central peak mediated by two shoulders at high and low field [27,28].

Fig. 1b shows the ^{31}P-NMR spectrum obtained for a fully hydrated DNA:DDA:DLPC (1:1:1) sample. A fit to the experimental lineshape using the matNMR [29] is also included. As expected, a superposition of an axially symmetric tensor for the phospholipid membrane and an axially asymmetric tensor for the DNA molecules can be fitted to the experimental spectrum. From the principal components estimated in the fitting procedure, we obtain $\delta_{aniso}=-74$ and $\eta=0.65$ which can be compared to $\delta_{aniso}=-108$ and $\eta=0.6$ obtained for solid fibers of Na–DNA [27]. It is unclear whether the reduction of δ_{aniso} is a result of different DNA conformations in the fibrous and intercalated forms, or if some limited motion of the DNA molecules results in narrowing of the ^{31}P spectrum.

For ^{31}P spectra of phospholipids one normally refers to the CSA as:

$$\Delta\sigma = \sigma_{\parallel} - \sigma_{\perp}, \quad (5)$$

where $\sigma_{\parallel}$ is the principal component for the parallel orientations (δ_{zz} in this convention) and $\sigma_{\perp}$ the perpendicular component. In liquid ordered phospholipid bilayers, where reorientation around the molecular axis is the only mechanism of averaging, $\Delta\sigma$ can be of the order of 100 ppm [30]. For the same phospholipid in the liquid disordered phase, where the molecular axis is rapidly moving with respect to the bilayer normal, $\Delta\sigma$ is reduced about 50%. Diffusion along a curved bilayer leads to further averaging of the ^{31}P CSA tensor and for vesicular dispersions of phospholipids in the liquid disordered state one typically obtains $\Delta\sigma \sim 40$ ppm [26,31]. For the phospholipid component in the DNA:DDA:DLPC (1:1:1) sample we obtain $\Delta\sigma=60$ ppm which is consistent with a liquid disordered phospholipid bilayer. Qualitatively the same results were obtained for the DNA:DDA:DLPC (1:1:0.5) system however, due to the fact that the phospholipid amount in the sample is low, the signal-to-noise ratio was rather poor even after acquiring for more than 24 h.

3.2. Local and long range mobility

A question of interest in the dynamics of this concentrated system is how the mobility of the charged and uncharged lipid is altered by the presence of DNA. A fluid lipid mixture typically displays a unique lateral diffusion coefficient unless other species like proteins or cholesterol is added [32–34]. There is an electrostatic reason for the cationic lipid to restrict its motions around the DNA molecules while the zwitterionic molecules move more freely between DNA molecules [24]. Experimental support of this suggestion is still lacking. In fact, molecular dynamics simulations indicate that both lipids are involved in neutralizing DNA [35]. In Monte Carlo simulations, demixing could be observed for a membrane constituted of cationic and anionic lipids [36], this feature was experimentally observed for a membrane containing cationic lipids and negatively charged fluorescently labeled lipids [37].

We have studied the molecular order and dynamics of this system on two scales: local reorientations and translational mobility on the 1–100 μm length scale, both represented in Fig. 1c. Local mobility comprise many modes of motion like vibrations, rotation of chemical groups or the entire molecule about its

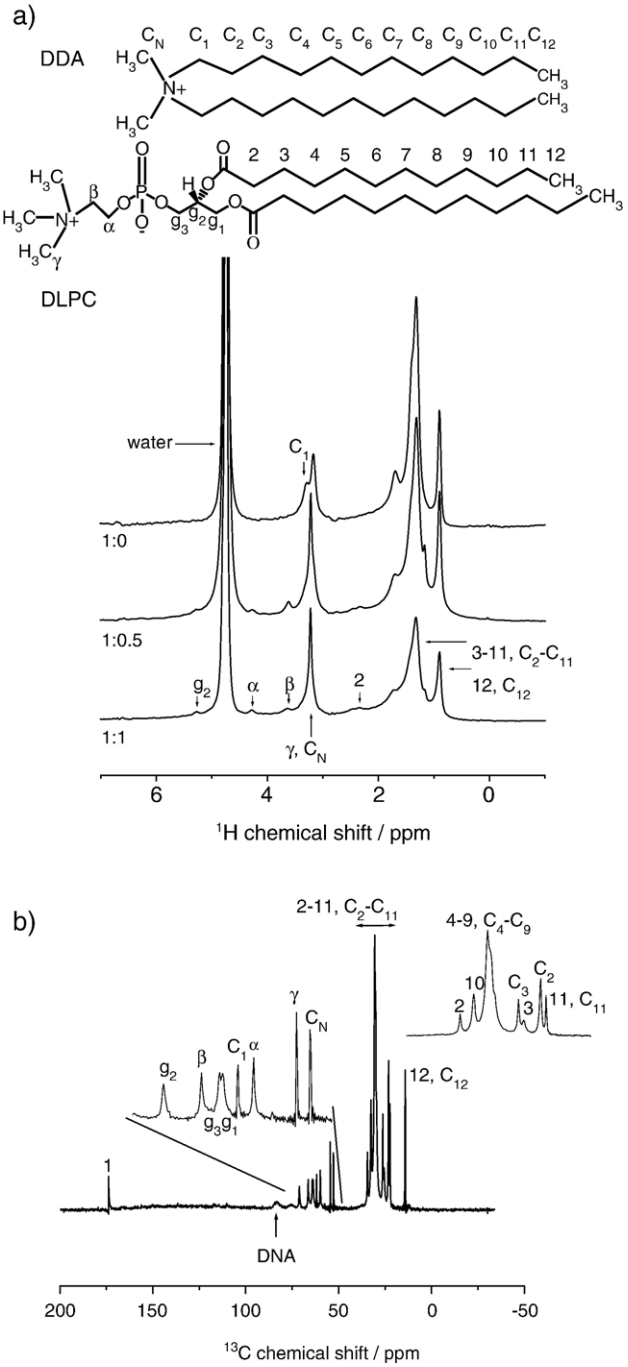

Fig. 3. (a) Single-pulse ^{1}H MAS spectra at 400 MHz, 5 kHz spinning speed of fully hydrated, isolectric DNA:DDA:DLPC precipitates; from bottom to top (mol ratios): 1:1:1, 1:1:0.5 and 1:1:0. The major peaks arise from water at 4.7 ppm, DLPC and DDA headgroups at 3.2 ppm, DLPC and DDA hydrocarbon tails at 1.5 ppm and from the end methyl group in both lipid tails at 0.9 ppm (see structure of the lipids in the inset). (b) ^{13}C CP-MAS spectrum of isolectric, fully hydrated DNA:DDA:DLPC (1:1:1) precipitate at 5 kHz spinning speed. Several narrow peaks originating from the lipid hydrocarbon tails and lipid headgroups are resolved in the 0–50 ppm and 50–75 ppm range, respectively. A broader peak from the DNA sugar groups is also resolved at 83 ppm.

principal molecular axis or, generally, conformational rearrangements. In this rather complicated system with a mixture of lipids and DNA, the mobility associated with different molecules can be intricate to unravel but solid-state NMR techniques turned out to be useful because motions of different parts in the molecules could be resolved. Diffusion NMR yields information about the translational mobility on the 10–1000 ms time scale and 1–100 μm length scale. Complications in the interpretation of the data can arise if the sample is inhomogeneous in the same length scale. For this reason, the particle morphology was studied using electron microscopy.

3.3. Electron microscopy

Scanning and Transmission Electron Micrographs (SEM and TEM) of the DNA–lipid precipitate are shown in Fig. 1d. The grains are porous and of many different sizes. At higher magnification we can observe a layered structure composed of many long and thin flakes. The stripes observed in the TEM image of the particle categorize as Moiré patterns, which are commonly observed in superimposed polymer lamellar crystals [38,39]. There are two fundamentally different types of Moiré interference: translation (due to spacing difference between two sets of parallel planes) and rotation (due to rotation of sets of planes with the same spacing) [40]. In contrast to SAXS, the Moiré pattern cannot give information about the spacing in the lamellar DNA–lipid precipitate. Nevertheless, this image indicates that the domains of the lamellar phase in a precipitate particle are randomly superimposed. When we image a thinner sample with just one layer of ordered lamellar structure, the density function of that image gives a distance of roughly 60 Å which agrees with the SAXS data (see above).

3.4. Solid-state NMR

The linewidth of a ^{1}H spectrum of a liquid-crystalline lamellar assembly is determined by a number of interactions scaling as $(3\cos^2\theta-1)$, where θ is the angle between the normal to the lamellar plane and the magnetic field. These interactions include mainly intramolecular ^{1}H–^{1}H dipolar couplings, chemical shift and magnetic susceptibility anisotropy (chemical exchange and small heteronuclear dipolar couplings can also affect the width of the spectra). Mobility over various length scales like conformational changes, rotation of a molecule around its principal axis, lateral molecular diffusion along the aggregate, rotation of the entire aggregate and even deformations in the aggregate towards higher surface area [19] contribute to the averaging of intramolecular dipolar couplings. In order to induce narrowing, the time scale for the motion has to be shorter than the inverse of the strength of the interaction (in Hz). Although it is often difficult the extract detailed information about what type of motions contribute to the narrowing, the ^{1}H linewidth is still a good measure for the general "mobility" and how it is changing as a function of external conditions [11].

MAS experiments rely on the fact that broadening of the NMR resonance lines can be substantially decreased if the sample is rotated while being inclined relative to the magnetic field at an angle that eliminates the $(3\cos^2\theta-1)$ factor. If the sample is spun at the magic angle (54.7°) at a speed (in frequency units) exceeding the strength of the interactions, high-resolution ^{1}H spectra are achieved [41,42].

In Fig. 3a, we show ^{1}H MAS spectra obtained at 5 kHz for three different DNA:DDA:DLPC precipitates with increasing amount of DLPC from top to bottom (see structure of both lipids in inset). The DNA peaks are much too broad to be seen in this spectral window so all the signals arise from water and from

Table 1
Summary of the results obtained for three DNA:DDA:DLPC precipitates (1:1:0, 1:1:0.5 and 1:1:1)

Assignment	^{13}C shift (ppm)			^{1}H shift (ppm)			^{1}H T_2^*(ms)			$\lvert S_{CH}\rvert$
	1:1:0	1:1:0.5	1:1:1	1:1:0	1:1:0.5	1:1:1	1:1:0	1:1:0.5	1:1:1	1:1:0.5
12, C_{12}	14.2	14.2	14.2	0.9	0.9	0.9	2.6	2.0	2.0	0
11, C_{11}	22.3	22.3	22.3	1.5	1.5	1.5	1.5	1.2	1.0	0
C_2	23.0	23.0	23.0	1.4	1.4	1.4	1.6	1.8	1.3	0.07
3	–	25.4	25.5	–	1.5	1.5	–	1.3	1.1	0.17
C3	26.2	26.2	26.2	1.4	1.4	1.4	2.1	1.5	1.3	0.07
4–9, C_4–C_9	30.2	30.5	30.6	1.3	1.3	1.3	1.8	1.4	1.1	0.15
10, C_{10}	32.4	32.5	32.5	1.3	1.3	1.3	1.9	1.6	1.2	0.10
2	–	34.5	34.5	–	2.3	2.3	–	1.1	0.9	0.2/0.12/0.07
C_N	52.6	52.7	52.8	3.2	3.2	3.2	2.4	1.7	1.3	0
γ	–	54.5	54.5	–	3.2	3.2	–	3.0	2.5	0
α	–	59.8	59.8	–	4.3	4.3	–	0.6	0.8	0.15
C_1	62.0	61.9	61.8	3.3	3.3	3.3	1.3	0.9	0.5	0
g_1	–	63.7	63.7	–	4.2	4.2	–	0.8	0.7	0.18/0.10
g_3	–	64.0	64.0	–	4.2	4.2	–	0.7	0.7	0.15/0.10
β	–	66.4	66.4	–	3.7	3.7	–	0.9	1.0	0.13
g_2	–	71.1	71.1	–	5.3	5.3	–	1.0	0.7	0.22
DNA sugar	75.7	75.6	75.3	–	–	–	<0.05	<0.05	<0.05	–
DNA sugar	83.2	83.4	83.4	–	–	–	<0.05	<0.05	<0.05	–
1	–	173.7	173.8	–	2.7	2.7	–	0.25	0.25	–

^{13}C, ^{1}H chemical shifts and ^{1}H linewidth T2∗are obtained in the WISE experiment. ^{1}H–^{13}C order parameters are obtained from the R-PDLF technique.

DDA and DLPC. By spinning at the moderate rate of 5 kHz we observe that the spectra are rather narrow. Peaks originating from the last methyl group in the hydrocarbon tails and the rest of the tail can be resolved; the peaks assigned to the headgroup of the lipids can also be resolved. This indicates that, with the exception of DNA, all molecules are rather mobile in the hydrated DNA–lipid precipitate. The use of the WISE technique to study dynamics relies on the fact that mobility information contained in ^{1}H spectra can be correlated with chemical specificity contained in ^{13}C spectra. This possibility is very important in this study, where the objective is to disentangle the mobility associated with DNA and two similar molecules (lipids) composing the aggregate. Fig. 3b shows the ^{13}C CP-MAS spectrum of the DNA:DDA:DLPC (1:1:1) precipitate. Two broad peaks at 75 and 83 ppm originate from the sugar groups of the DNA. These peaks get a bit sharper with stronger ^{1}H decoupling, but still remain rather broad (data not shown). Since the ^{13}C chemical shift is sensitive to molecular conformation, the width of the sugar peaks indicates that the DNA is quite disordered. A multitude of lipid peaks can be resolved and the peak assignment for all the samples is given in Table 1. The resolution obtained in the ^{13}C spectra allows us to distinguish between all the peaks for each lipid headgroup and even two carbons in the hydrocarbon tails (2, C_2 and 3, C_3) can be separated. For every resolved ^{13}C resonance in Fig. 3b, a ^{1}H spectrum reflecting the dipolar couplings among the protons in the proximity of the respective ^{13}C nuclei can be acquired. In other words, correlation of chemical structure and segmental mobility can be obtained. One way of doing this kind of two dimensional NMR experiment is the so-called WISE [11] method (see Fig. 2a) where an incremented ^{1}H evolution period, t_1, is applied between the initial ^{1}H excitation pulse and ^{1}H–^{13}C cross polarization; ^{1}H evolution can be detected as an amplitude modulation of the ^{13}C peaks. Time domain fitting of the ^{13}C peak area vs. t_1 to an exponentially damped cosine function yields estimates of T_2^*, which in this case is a measure of the ^{1}H dipolar linewidth, and the ^{1}H chemical shift [19]. The uncertainty of the fit was assessed using the Monte Carlo method by Alper and Gelb [43]. Except for carbons 1 and C_1 of DLPC and DDA respectively, which both suffer from instability of the peak phase, the errors associated with T_2^* and chemical shift determination was 5–10% and 1%, respectively. The T_2^* values associated with the ^{13}C peaks are included in Table 1. With exception of the static DNA molecules which decay faster than 50 μs, T_2^* for the lipids in the DNA–lipid aggregate are in the range of 0.5–3 ms, indicating that they are rather mobile. Similar results were obtained previously for another kind of DNA–lipid precipitate possessing hexagonal structure [19]. Increasing the DLPC content in the DNA:DDA:DLPC precipitates results in shorter T_2^* for the hydrocarbon tails and for

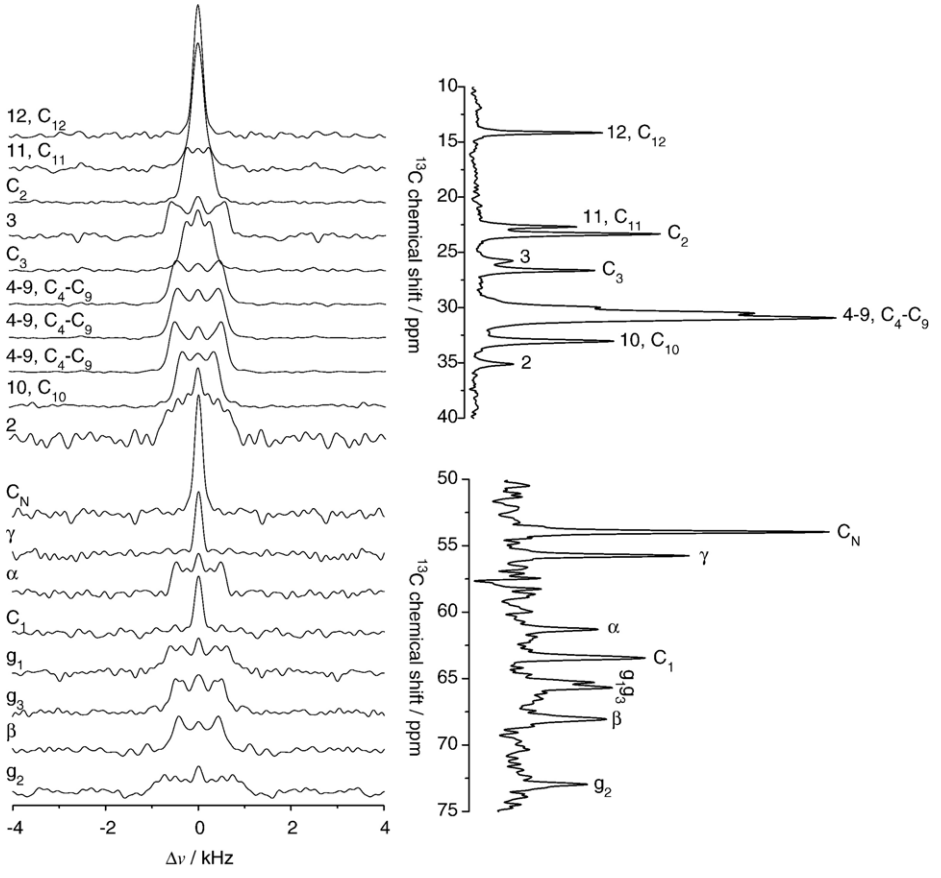

Fig. 4. Dipolar cross-sections through a 2D R-PDLF spectrum of the fully hydrated DNA:DDA:DLPC (1:1:0.5) precipitate. The 1D ^{13}C MAS spectrum is shown to the right. Several splittings can be observed mainly for the lipid hydrocarbon tail region and a few for the headgroup region of DLPC. The dipolar spectra are symmetric as a result of recording data sets which are cosine modulated in the indirect dimension.

the headgroups of DDA and DLPC. General to all systems is that the T_2^* for sites C_2 and C_3 in the DDA chain are longer than the equivalent 2 and 3 sites of the DLPC chain. DNA interaction with the lipid bilayer induces more mobility on the DDA chain than on the DLPC chain. Assuming that the model presented in Fig. 1a is correct, with the cationic DDA headgroups being in closer contact with DNA than the zwitterionic DLPC headgroups, one should expect a higher perturbation of lipid packing for DDA than for DLPC. T_2^* for the methyls of the headgroups are 3 ms for DLPC (γ) and 1.7 ms for DDA (C_N). However, due to the structure of the headgroup of the different lipids, one cannot justify the differences in T_2^* exclusively on the fact that DNA makes C_N in DDA less mobile than γ in DLPC. The charged N+ group in DLPC is freer to rotate due to the single alkyl chain–N bond while in DDA, N+ is bonded directly to two carbons of the hydrocarbon tail. It is also possible that the tilt angle of the zwitterionic headgroup is influenced by the electrostatics as previously observed for an equivalent lipid mixture without DNA by Lindström et al. [44].

Another observation common to all DNA:DDA:DLPC precipitates is that the ratio T_2^*(headgroup)/T_2^*(tails) >1 at high hydration and <1 at low water content (data not shown); we also observed this feature in a previous study of a hexagonal DNA-surfactant precipitate [19].

The ^{1}H linewidth is a good mobility probe, but the majority of structural and dynamic NMR studies of liquid-crystalline materials have in the past been performed using ^{2}H NMR [45]. The ^{2}H quadrapolar interaction provides information about C–^{2}H segmental mobility via the width and the shape of the spectrum. A major drawback of ^{2}H NMR spectroscopy is the need for isotopic labeling of the system. Moreover, the peak assignment of one-dimensional ^{2}H spectra of systems with many ^{2}H sites can be complicated. The spatial dependence of the ^{2}H quadrapolar interaction tensor is identical to that of the ^{13}C–^{1}H dipolar tensor. Thus, an alternative approach to investigate liquid-crystalline systems is to measure ^{1}H–^{13}C dipolar couplings by SLF spectroscopy. This latter method has the great advantage that isotopic labeling is not required. The structure and dynamics in lamellar liquid-crystalline phases of phospholipids have been explored with SLF techniques, and a very good agreement between the local order parameter calculated by the ^{1}H–^{13}C dipolar splittings and by the traditional ^{2}H quadrupolar splittings was observed [22,46]. The measured dipolar or quadrupolar splittings are commonly converted to the order parameter

$$S_{CH} = \left\langle \frac{3\cos^2\theta - 1}{2} \right\rangle, \tag{6}$$

where θ is the angle between CH bond and the main magnetic field, and the angular brackets denote an average over all molecular conformations on a time scale shorter than the inverse of the relevant NMR interaction (in Hz). For ^{1}H–^{13}C dipolar couplings, $|S_{CH}|$ is calculated through [22]

$$|S_{CH}| = \frac{\Delta\nu_d}{21\ \text{kHz}}, \tag{7}$$

where $\Delta\nu_d$ is the measured dipolar splitting.

Fig. 4 displays ^{1}H–^{13}C dipolar slices extracted from a 2D R-PDLF spectrum of a DNA:DDA:DLPC (1:1:0.5) complex. Many splittings can be observed for the different sites in both lipid molecules. The 2D recoupling experiment is very sensitive, for instance, peaks that are not fully resolved in the ^{13}C dimension (4–9, C_4–C_9) still give rise to a series of splittings. Most of the lipid CH_2 groups produce only one dipolar splitting. This shows that rapid axial diffusion in combination with internal bond rotations, renders the two ^{1}H–^{13}C couplings identical, even though they are strictly inequivalent. A few segments, however, exhibit additional features. For example, the g_1 cross-section shows two splittings which demonstrates that the motion of this CH_2 group results in inequivalent ^{1}H–^{13}C dipolar interactions. Furthermore, the dipolar slice taken from the 2 position contains three splittings. As discussed elsewhere [22], this shows that the two acyl chains in DLPC behave differently. The estimated order parameters are compiled in Table 1. The end of the hydrocarbon tails and the headgroups do not give rise to any splitting. The splittings that we obtain for the hydrocarbon tail region (4–9, C_4–C_9) are considerably smaller than the ones obtained for the pure phospholipid case [22]. This implies that the presence of DNA provides an environment that allows for more averaging of the ^{1}H–^{13}C dipolar interaction. Choosakoonkriang and co-workers [10] suggest that the alignment of the lipid headgroups with DNA alters the packing of the lipid molecule, and that there is an increased disorder in the alkyl chain. Additional averaging can arise due to the fact that DNA induces undulations on the lipid membrane [47]. Molecular displacements over an uneven surface would lead to a reduction in the magnitude of the ^{1}H–^{13}C dipolar splitting.

Cationic/zwitterionic lipid mixtures were previously studied by Huster et al. [48] using ^{2}H NMR experiments in order to observe how the lipid chain order is influenced by the lipid composition and the addition of anionic polyelectrolyte. In the absence of polyelectrolyte the average order parameter of the lipid chains remains nearly unchanged for all cationic/zwitterionic lipid ratios. When anionic polyelectrolyte is added, there is a preferential interaction with the cationic lipid and the order parameter is changing for different amounts of cationic lipid.

The R-PDLF experiment corroborates the WISE experiment for sites C_3 and C_2 (DDA) and equivalent 3 and 2 (DLPC). The zwitterionic DLPC sites produce splittings of twice the magnitude as the splittings exhibited by the equivalent sites in cationic DDA. This indicates that, due to the charge nature of the lipid headgroups, DDA molecules are more perturbed by DNA electrostatic forces leading to an increased disorder of the CH_2 segments close to the headgroup in comparison with the equivalent sites on DLPC.

Fig. 5a depicts the ^{1}H linewidth (expressed as $1/T_2^*$) and the ^{1}H–^{13}C order parameters from the headgroups to the hydrocarbon chains for one of the DNA:DDA:DLPC precipitates. For the sites in the tails that cannot be resolved we assign the same value to each site. No $1/T_2^*$ value is given for site 1 in the DLPC since it contains no directly bound ^{1}H. The observed signal for this site originates from several more remote ^{1}H, and is consequently not well described with the exponentially damped cosine function. Some points not connected correspond to sites

that produce more than one splitting. $1/T_2^*$ and $|S_{CH}|$ follow the same trend for DDA and DLPC lipid molecules.

The mobility/order of DDA and DLPC hydrocarbon chains can be compared at sites C_2, 2 and C_3, 3. The order parameters for DLPC at these sites are larger than those for DDA. The average length $\langle L\rangle$ of the hydrocarbon tails relative to the all-*trans* state can be estimated using the segmental order parameters S_{CH} [49,50] as:

$$\langle L\rangle = l_0\left[\left(\frac{n-m+1}{2}\right) - \sum_{i=m}^{n-1} S_{CH}^{(i)} - 3S_{CH}^{n}\right], \quad (8)$$

where l_0=1.25 Å is the length of a C–C bond projected onto the axis of the all-*trans* reference state, n is the number of carbons on the lipid acyl chain (n=12 for DLPC and DDA) and m is the position of the carbon closest to the headgroup. In a phospholipid, one defines m=2 for the *sn*-1 chain and m=3 for *sn*-2 [51]. From the average chain length one can also estimate the average cross-sectional area of the acyl chain as

$$\langle A\rangle = V_{chain}/\langle L\rangle. \quad (9)$$

The volume of the chain length, V_{chain} can be defined by the volume per methylene group and is given by [49]

$$V_{chain} = n'V_{CH_2} + V_{CH_3} \cong n'V_{CH_2} + 2V_{CH_2}, \quad (10)$$

where $n'=n-m$ is the number of segment units used to calculate the average projected length and V_{CH2}=28.0 Å^3. Here only the order parameters for positions 2 and 3 can be resolved individually for DLPC and DDA together with a common splitting obtained for positions 4–9. Nevertheless, we can attempt to estimate the lengths of the DDA and DLPC chains taking into consideration only the part of the acyl chain closest to the headgroup region. In fact, the model for the estimation of areas/lipids using the order parameters profiles assumes that only the carbons nearest to the headgroup reflect the molecular area at the lipid/water interface [51,52], e.g. for a DPPC (n=16) lipid only the order parameters in the plateau region (n=10) of the order parameter profile is taking into account. If we calculate the average lengths assuming n=5, we obtain $\langle L\rangle^{DLPC}$=3.7 Å and $\langle L\rangle^{DDA}$=3.3 Å. These values result in chain cross-sectional area of $\langle A\rangle^{DLPC}$=37 Å^2 and $\langle A\rangle^{DDA}$=42 Å^2, i.e. 15% larger area for DDA. In a pure phospholipid bilayer phase, this is the increase typically observed by increasing temperature. The average cross-sectional area per chain goes from 36 Å^2 to 40 A^2 by increasing the temperature from 40 °C to 80 °C [51]. In order to properly calculate the area per chain one should ideally have access to the entire order parameter profile for each chain and here we make an estimate based on solely two carbons. Nevertheless, we do have indications, as well as is reported evidence [48], that the complexation of DNA (or any anionic polymer) to a cationic/zwitterionic lipid bilayer does induce an

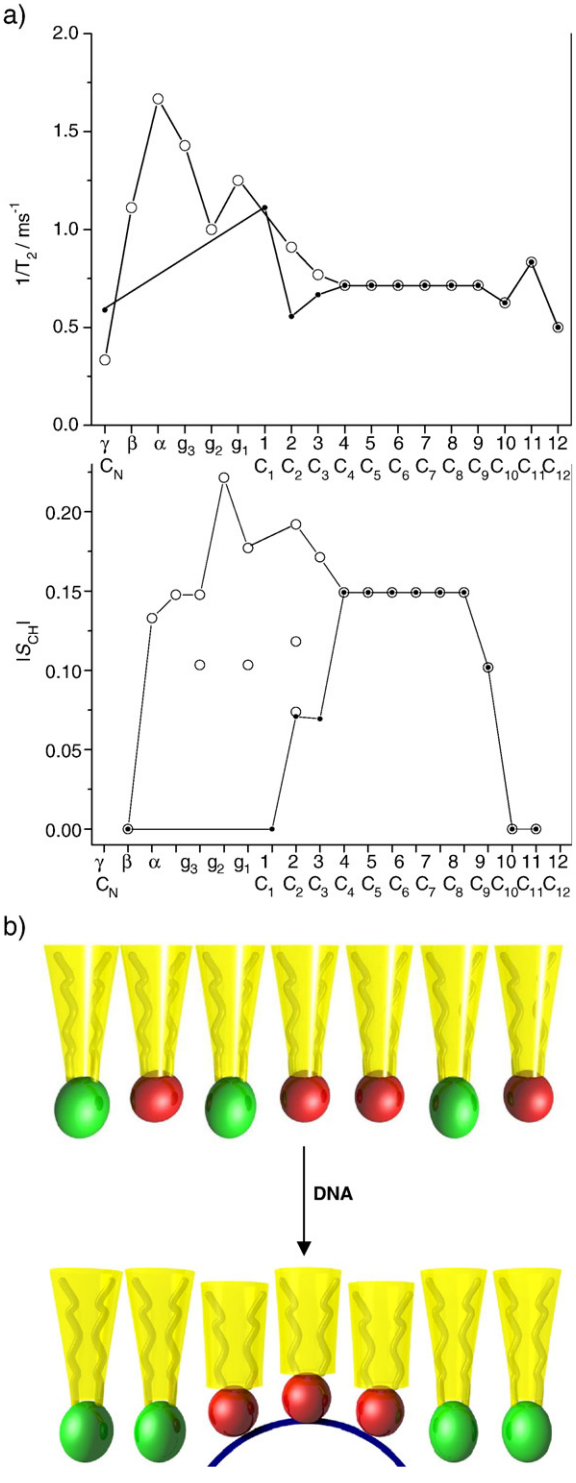

Fig. 5. (a) ^{1}H dipolar linewidth, expressed as $1/T_2^*$, (top) and ^{1}H–^{13}C order parameters, $|S_{CH}|$ (bottom) associated with every resolved ^{13}C resonance line for the DNA:DDA:DLPC (1:1:0.5) precipitate (open circle: DLPC and solid circle: DDA). For unresolved positions (4–9 and C_4–C_9) the same value was assigned to all carbons. The unconnected points at sites g_3, g_1 and 2 correspond to multiple splittings associated with the same segment. The $1/T_2^*$ for site 1 in DLPC was not included due to the large error associated with the fitted values. $1/T_2^*$ and $|S_{CH}|$ follow the same trend: C_2 and C_3 (DDA) segments are more mobile/disordered than the equivalent 2 and 3 (DLPC) due to stronger electrostatic interaction of DDA headgroup with DNA. (b) Tentative illustration of lipid packing in the lamellar phase before (top) and after (bottom) DNA interaction. The red spheres represent the DDA headgroups and the green ellipses the DLPC headgroups. The close interaction of DNA with DDA results in a shorter effective chain length for DDA. (For interpretation of the references to colour in this figure legend, the reader is referred to the web version of this article.)

asymmetric order profile for each lipid acyl chain. Furthermore, while the DLPC chains display order parameters close to the headgroup that are "normal" in bilayer phases (around 0.2), DDA displays abnormally low order parameters at this point. Smaller order parameters are translated into an effectively shorter chain length and consequently increased cross-sectional area per chain. Molecular dynamics simulations would be highly useful for elucidating which intermolecular forces are responsible for the experimentally observed perturbations of the DDA hydrocarbon chains close to the headgroup. If we are allowed to speculate, Fig. 5b illustrates a possible mechanism of the effect of DNA on the DDA/DLPC lipid membrane. The electrostatic preference of DNA for DDA combined with geometrical constraints could lead to a reduction of the DDA chain length in comparison to DLPC, resulting in an increased cross-sectional area per chain and consequently larger amplitude for conformational changes of the DDA chain.

3.5. Diffusion NMR

The molecular diffusion was measured under non-spinning conditions with the PFG STE experiment shown in Fig. 2c. The echo intensity I for an ensemble of spins with an isotropic diffusion coefficient D, longitudinal relaxation time T_1, and transverse relaxation time T_2 is given by [53]

$$I = \frac{I_0}{2}\exp\left(-\frac{2\tau_1}{T_2} - \frac{\tau_2}{T_1} - bD\right) \tag{11}$$

where $b=(\gamma G\delta)^2(\Delta-\delta/3)$ and I_0 is the signal intensity after a single 90° pulse. The experiment is performed by recording I for a series of G at constant values of τ_1, τ_2, δ, and Δ. A plot of $\log(I)$ vs. b, a so-called Stejskal–Tanner plot, yields a straight line where D is given by the slope.

For anisotropic systems, T_1 and T_2 will in general depend on the average molecular orientation with respect to the main magnetic field, and D on the direction of the magnetic field gradient. The orientation of a lamellar system is described by the angle θ between the axis of cylindrical symmetry and the coincident directions of the main magnetic field and the applied field gradient. Let us first assume that the sizes of the lamellar domains are large with respect to the maximum displacement during the diffusion time. The observed diffusion coefficient for a macroscopically oriented system is

$$D_\theta = D_\parallel \cos^2\theta + D_\perp \sin^2\theta \tag{12}$$

where $D_\parallel$ and $D_\perp$ are the self-diffusion coefficients parallel and perpendicular to the lamellar plane normal. Neglecting relaxation, the signal from an ensemble of randomly oriented domains can be written as [14]

$$I(b) = I_{G=0}\exp(-bD_\perp)\int_0^1 \exp[-b(D_\parallel - D_\perp)x^2]\mathrm{d}x \tag{13}$$

giving rise to a characteristic multiexponential decay in a Stejskal–Tanner plot [54,55].

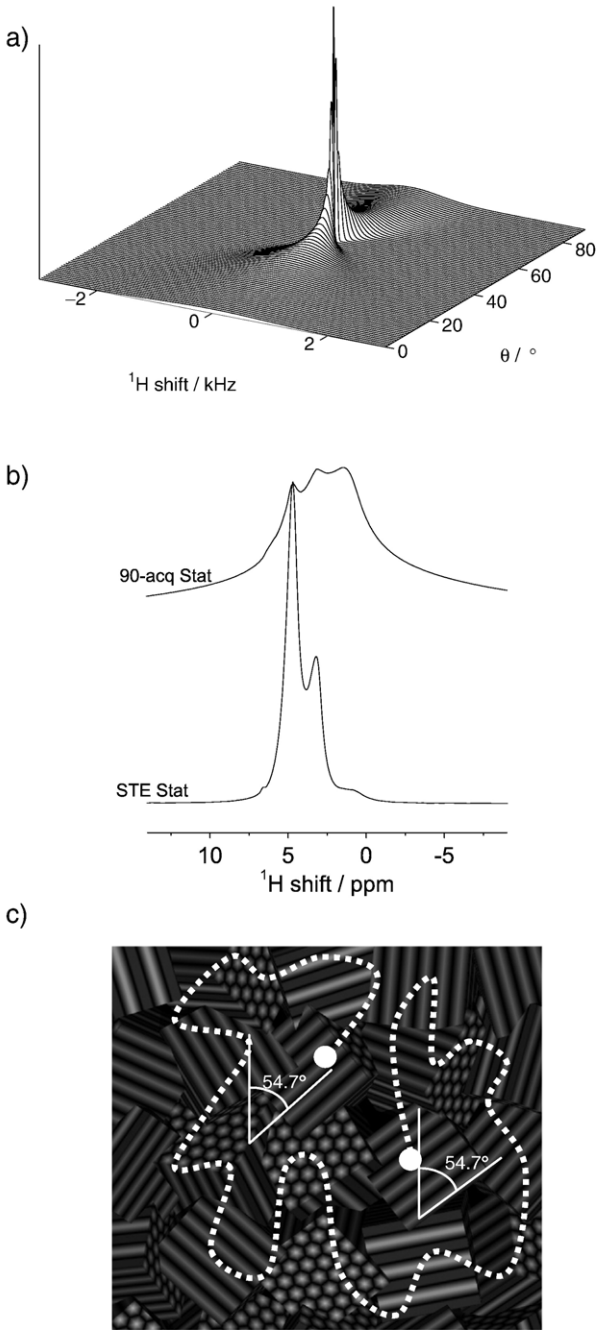

Fig. 6. (a) Simulated lipid ^{1}H lineshapes as a function of the angle θ between the magnetic field and the lamellar director. The linewidth is given by Eq. (14). The narrowest line is observed at the magic angle 54.7°. (b) Static ^{1}H spectra for a single pulse (90-acq Stat) and a Stimulated Echo (STE Stat) experiment for the DNA:DDA:DLPC (1:1:1) precipitate hydrated with D_2O. The widths of the lipid peaks are significantly reduced in the STE experiment as only domains oriented close to the magic angle 54.7° contribute to the signal. (c) Schematic illustration of a molecule diffusing over a number of many small domains randomly oriented at different angles. During the diffusion time, the molecules sample a large number of domains oriented at all angles. The signal in the STE experiment originates from lipid molecules that are located in domains oriented at the magic angle during both τ_1 periods. No such restriction applies during the τ_2 period since T_1 is independent of orientation.

Rapid molecular diffusion in a liquid crystal leads to an effective averaging of all the intermolecular dipolar couplings. Also the intramolecular dipolar couplings are partially averaged. Because of the cylindrical symmetry, the only surviving components of the dipolar interactions are parallel to the axis of symmetry [56]. The resonance line for a randomly oriented sample is a superposition of lines with equal shape, but with the width scaled by $(3\cos^2\theta-1)/2$ as shown in Fig. 6a, leading to the characteristic super-Lorentzian lineshape [57]. When phrased in terms of relaxation this fact can be expressed as

$$\frac{1}{T_{2,\theta}} = \frac{1}{T_{2,\theta=0}}\left|\frac{3\cos^2\theta - 1}{2}\right| + \frac{1}{T_2} \tag{14}$$

where T_2 is the "true" relaxation time and $1/T_{2,\theta=0}$ is the maximum contribution from the residual intramolecular dipolar couplings. For reasons related to the hardware generating the pulsed field gradients, the minimum value of τ_1 in the STE sequence is about 1 ms. For many lamellar systems $T_{2,\theta=0}$ is much smaller than this value, leading to the loss of signal from domains oriented at other angles than the magic angle 54.7° where the first term in Eq. (14) vanishes. As an example, a spin echo experiment performed under non-spinning conditions gave the results $T_{2,\theta=0}$=30 μs and T_2=3 ms for the DNA:DDA:DLPC (1:1:1) system (data not shown). T_1 relaxation depends on magnetic field fluctuations on the frequency scale of the Larmor precession. The orientational variation of T_1 can therefore be neglected for typical lyotropic liquid crystals [57]. Diffusion experiments performed under such conditions would lead to a single exponential decay in the Stejskal–Tanner plot with an effective D given by inserting 54.7° into Eq. (12).

The presence of the magic-angle effect for the samples studied here is shown by the ^{1}H spectra in Fig. 6b. The resonance lines in the spectrum acquired after a single excitation pulse contain both narrow and broad components. The spectrum obtained with the STE sequence contains, in addition to the narrow water signal, only components originating from lipids in domains oriented close to the magic angle. The main contribution to the linewidth in this case is the difference in magnetic susceptibility between the precipitate grains and the surrounding D_2O phase (cf. Fig 1d), leading to microscopic magnetic field inhomogeneity. This inhomogeneous broadening is removed with MAS as shown in Fig. 3. Unfortunately, MAS is not easily combined with the high-gradient diffusion experiments necessary to study the rather slow lipid diffusion in these systems.

No deuterium quadrupolar splitting could be observed for the DNA:DDA:DLPC hydrated with D_2O at 99.5% RH (no excess), indicating that the sample is constituted of small domains [58]. Lasic and co-workers [59] used the lineshape of the first-order reflection in the SAXS spectra of a lamellar complex consisting of DNA and a mixture of DDAB and cholesterol; the domain size was estimated to be around 35 nm. We also have microscopy indications that the lamellar domains in our study are superposed and randomly oriented (see Fig. 1d). If we assume a lipid diffusion coefficient of 2×10^{-11} m^2/s, a diffusion time of 0.1 s corresponds to typical molecular displacements of about 1 μm, i.e. much larger than the expected domain size. This has the important effect that the system appears isotropic on the length scale given by the diffusion experiment. Molecules sampling a large number of domains during the diffusion time would result in a single exponential Stejskal–Tanner plot. The effective diffusion coefficient is then given by the principal components of the diffusion tensor and the details of the spatial distribution of the domains. A schematic of the diffusion in a system comprised of randomly oriented small domains is shown in Fig. 6c. Although the detected signal arises from molecules located in domains oriented close to the magic angle during both τ_1 periods in the STE sequence, the molecules are free to move over domains oriented at any angle during the τ_2 period which constitutes more than 95% of the total duration of the pulse sequence. Exchange experiments, which will be reported elsewhere [58], confirm that the lipids experience domains of many different orientations on a time scale shorter than 0.1 s. It should be emphasized once more that the system appears isotropic on the length scale defined by the diffusion experiment, and that each component then gives rise to a single exponential decay in a Stejskal–Tanner plot.

As shown in Fig. 6b, the spectroscopic resolution of the PFG STE experiment is limited. The observed ^{1}H NMR spectrum for the DNA:DDA:DLPC system consists of a number of overlapping peaks. The values of T_2^* estimated with the WISE experiment indicate that the two lipids contribute almost equally to the observed signal, while there is no contribution from the DNA. Despite the small concentration, the major component is actually residual protons in the water (D_2O), which is strongly favored because of its long T_2. Water in the saturated samples is located not only within the lamellar structure, but also outside the precipitate grains and between the flakes within one grain (cf. the electron micrographs in Fig 1d). The presence of several species with different diffusion coefficients gives rise to multiexponential signal decay, which can be written as

$$I(b) = I_{G=0}\int_0^\infty P(D)\exp(-bD)\mathrm{d}D \tag{15}$$

where $P(D)$ is a continuous distribution of diffusion coefficients. $P(D)$ is preferably estimated from experimental $I(b)$ data by assuming a functional form for the distribution [55]. For complex systems it is often necessary to resort to a general Inverse Laplace Transform (ILT) algorithm [60]. This method of analysis should be applied with great caution because of the non-uniqueness of the obtained solution. In addition, it is difficult to establish proper error estimates [61]. The solution stability is improved by recording many data points with high signal-to-noise ratios.

Stejskal–Tanner plots for DNA:DDA:DLPC with increasing amount of DLPC are presented in Fig. 7a. Because of the many components contributing to the signal, the data were analyzed with an ILT algorithm giving the distribution of the diffusion coefficients shown in Fig. 7b. The distributions consist of a region between 1×10^{-10} and 2×10^{-9} m^2/s originating from water in a number of different sites as explained above, and a region below 5×10^{-11} m^2/s with contributions from the lipids. Note that the data in Fig. 7a are normalized with respect to the

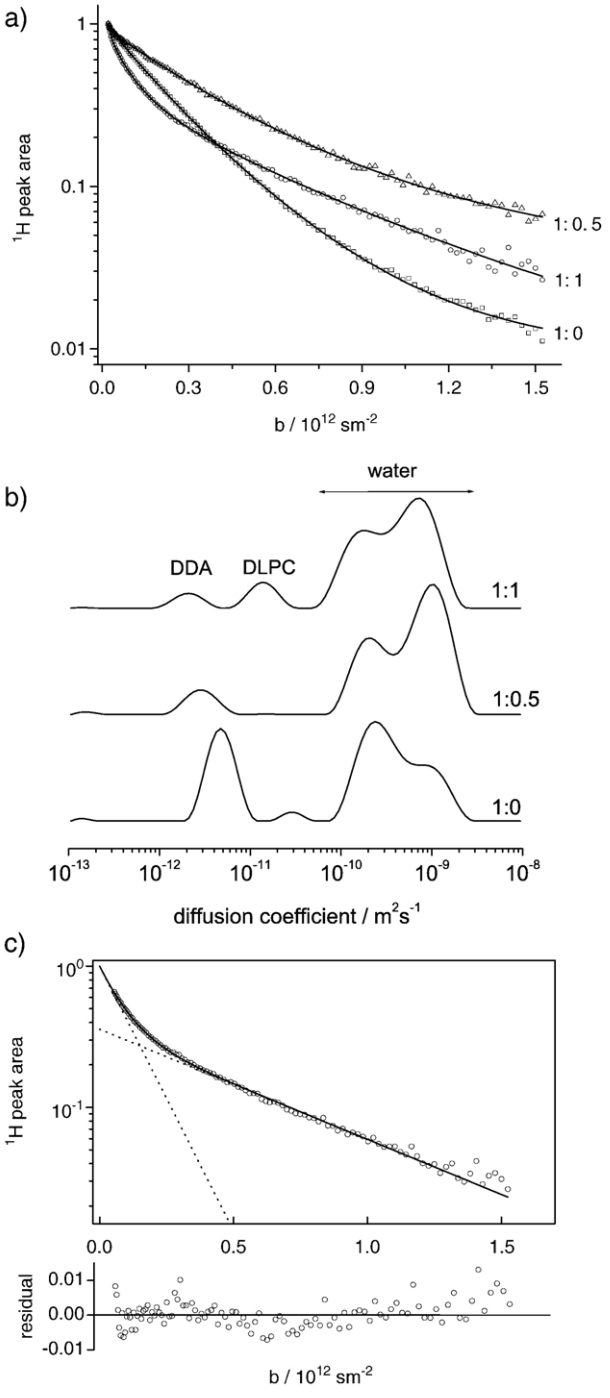

Fig. 7. (a) ^{1}H peak area vs. b in the PFG STE diffusion experiment for D_2O saturated DNA:DDA:DLPC precipitates (1:1:0, 1:1:0.5 and 1:1:1). The curves are normalized to exclude the fast decaying signal originating from water (residual ^{1}H in the D_2O). (b) Distribution of diffusion coefficients as obtained by inverse Laplace transformation. The sample containing equal amounts of DDA and DLPC (1:1:1) exhibits a bi-exponential decay indicating the presence of two components, one for DDA (slow) and another for DLPC (faster). The reduction of DDA diffusion upon addition of DLPC can be attributed to demixing in the plane of the lamellae. The non-linearity at high *b*-values for the DNA:DDA precipitate arises from the fact that the diffusion path is of the same size as the flake thickness in the precipitate grains. (c) Bi-exponential fit of the diffusion data for the 1:1:1 sample, verifying that the lipid diffusion can be described with two distinct components (1.8×10^{-12} and 1.2×10^{-11} m^2/s).

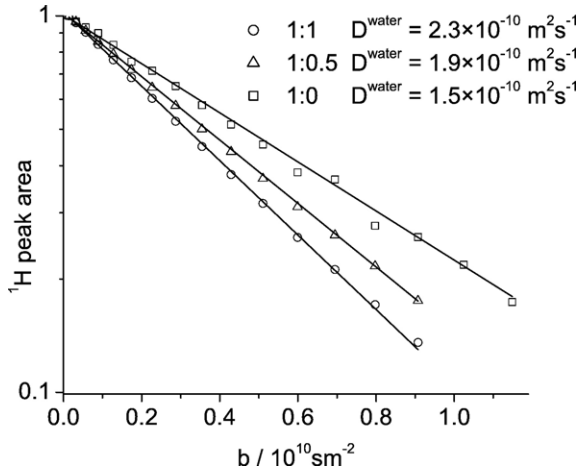

Fig. 8. ^{1}H peak area as a function of *b* in the water (H_2O) diffusion experiment for DNA:DDA:DLPC precipitates (1:1:0, 1:1:0.5 and 1:1:1) equilibrated at 99.5% relative humidity. Water diffusion is decreasing as the DLPC content is reduced.

signal from the lipids. The few data points containing contributions from water at low values of *b* are located outside the scale of Fig. 7a. The lipid diffusion coefficients are within the range usually obtained for pure lamellar phases of lipids without DNA [62]. This behavior is quite different from the very slow diffusion, below 10^{-13} m^2/s, observed for a hexagonally arranged DNA–cationic surfactant complex [19]. For the sample with equal amounts of DDA and DLPC (1:1) there is clearly a bi-exponential echo decay (neglecting the fast initial decay from water) and two distinct components (about 2×10^{-12} and 2×10^{-11} m^2/s) can be separated in the distribution obtained with the ILT. In order to verify the results from the ILT analysis, data in the *b*-range from 5×10^{10} to 1.5×10^{12} s/m^2 were fitted using a bi-exponential function as shown in Fig. 7c. The electrostatic interactions between DNA and DDA are expected to reduce the long-range mobility of DDA. For this reason we assign the slow component to DDA.

The echo decay curve for the DNA:DDA complex shows an intriguing curvature in the end. As described above, the lamellar domains are much smaller than the typical diffusion displacement, implying that a single component would give rise to a single exponential decay. The observed curvature is probably the result of the morphology of the sample grains. As shown in Fig. 1d, the DNA:DDA:DLPC grains display a layered morphology where each flake has a thickness of about 1 μm — the same size as the displacements during the diffusion time. Molecules located in μm-size flakes oriented perpendicular to the gradient would experience restricted diffusion, which is another cause of multiexponential signal decay [14].

For the sample with 1:0.5 molar ratio between DDA and DLPC, the ILT analysis did not yield any component at the expected value for DLPC. This fact is probably related to the problem of resolving two adjacent components with very different amplitude using the ILT method.

There is a trend of decreasing diffusion of DDA when increasing the amount of DLPC. The presence of DNA breaks the cylindrical symmetry of the lamellar phase. Let us denote

the directions parallel and perpendicular to the DNA by x and y, respectively. For the DNA:DDA system the bilayers are composed of pure DDA which is expected to move with equal rate in the x and y directions. If the lipids in the DNA:DDA:DLPC system are segregated, the inhomogeneous lipid concentration in the y-direction leads to reduced diffusion. In the limit of complete segregation the only diffusion would take place in the x-direction. The transition from two-dimensional diffusion for the pure DDA system to one-dimensional diffusion in a completely segregated DDA:DLPC system would lead to a factor of 2 reduction in the macroscopically observed diffusion. Such a change is actually observed in Fig. 7b. However, other alternative explanations for the reduced DDA diffusion can be considered. For example, from the discussion above it is clear that the molecules move across many domains with different orientation during the diffusion time. There is no information about the nature of the boundaries between the different domains, e.g. if the change of domain orientation occurs smoothly or abruptly, or if the bilayers and DNA helices extend across the domain boundaries. Increasing amount of DLPC could lead to a change in the domain boundaries or the spatial distribution and morphology of the domains. All these factors could influence the long-range diffusion. However, the important result of the diffusion experiments is the observation that DNA induces two different diffusion coefficients in a cationic/zwitterionic lipid membrane (cationic-slow, zwitterionic-fast).

The dynamics of the system were further investigated by studying the water diffusion. Equilibrating the samples with normal water at 99.5% relative humidity avoids the problem of multicomponent water diffusion. The influence of the lipids was reduced by increasing the value of τ_1 in the STE sequence to 10 ms. The diffusion coefficients were evaluated by fitting Eq. (11) to the experimental data. The results are displayed in Fig. 8. Because of the hydration level and the choice of pulse program parameters, the values correspond to water incorporated within the supramolecular structure of the aggregate. In the lamellar DNA:DDA:DLPC complex, water is located between DNA molecules and the lipid bilayer, as DLPC content is increased there is an increase in the lamellar spacing and consequently the water diffusion coefficient is higher. The values of the water diffusion coefficients are of the same magnitude as usually found for lyotropic liquid crystals [54,63]. In the case of the bilayers intercalated with parallel DNA strands, assuming that both the bilayers and the DNA molecules are impenetrable obstacles, the only diffusion takes place in the x-direction. The macroscopically observed values of approximately 2×10^{-10} m^2/s then correspond to a microscopic diffusion coefficient of 6×10^{-10} m^2/s, which is just a factor of 4 lower than the value for bulk water. This fact shows that the water molecules are locally very mobile even in these concentrated systems with only about 10 water molecules per charge.

4. Conclusions

Solid-state and diffusion NMR techniques yield molecularly detailed information about nm- and μm-scale structure and dynamics in complex lipid systems with both liquid and solid components. In hydrated precipitates of lamellar DNA:DDA:DLPC, DNA is solid while the lipids are mobile. For the molecular segments where the DDA and DLPC yield separate ^{13}C peaks, the DDA tails display smaller ^1H–^{13}C dipolar couplings and ^1H $1/T_2^*$ values. This can be the result of the preferential electrostatic interaction between DNA and DDA headgroup leading to an increased perturbation of DDA packing. Two distinct lipid components are observed in the diffusion experiment — one with a typical value for lipid diffusion in a lamellar phase and another one with a factor ten slower diffusion. The fast and slow components are assigned to DLPC and DDA, respectively. Lipid segregation induced by DNA is also reflected in the observation that DDA (cationic) diffusion coefficient is reduced by a factor of two with the addition of DLPC (zwitterionic). This is explained by a change in the diffusion behavior of the cationic lipid from 2D (along and across the DNA's) in the complex without DLPC to 1D (just along the DNAs) when DLPC is incorporated. Generally, the presence of DNA leads to an increased local mobility of both lipid alkyl chains. This could be the result of DNA-induced undulations in the membrane providing an environment for more efficient averaging of the dipolar interactions.

Acknowledgments

This work was supported by the Swedish Research Council (VR) and the Carl Trygger Foundation. The authors acknowledge Håkan Wennerström for helpful discussions and Sergey Dvinskikh for help with the solid-state NMR experiments. SOAD is acknowledged for inspiration (C. L. and D. T.).

Appendix A. Supplementary data

Supplementary data containing SAX diffraction patterns and the fitting to the ^{13}C peak area vs. ^1H evolution time in the WISE experiment can be found, in the online version, at doi:10.1016/j.bbamem.2007.09.035.

References

[1] J.J.B. Cockburn, N.G.A. Abrescia, J.M. Grimes, G.C. Sutton, J.M. Diprose, J.M. Benevides, G.J. Thomas, J.K.H. Bamford, D.H. Bamford, D.I. Stuart, Membrane structure and interactions with protein and DNA in bacteriophage PRD1, Nature 432 (2004) 122–125.
[2] F. Jacob, S. Brenner, F. Cuzin, On the regulation of DNA replication in bacteria, Cold Spring Harbor Symp. Quant. Biol. 28 (1963) 329–348.
[3] A.A. Infante, W. Firshein, P. Hobart, L. Murray, A nuclear membrane-associated DNA complex in cultured mammalian cells capable of synthesizing DNA in vitro, Biochemistry 15 (1976) 4810–4817.
[4] P. Felgner, L.T.R. Gadek, M. Holm, R. Roman, H.W. Chan, M. Wenz, J.P. Northrop, G.M. Ringold, M. Danielsson, Lipofection: a higly efficient, lipid mediated DNA-transfection procedure, Proc. Natl. Acd. Sci. U. S. A. 84 (1987) 7413–7417.
[5] L.K. Medina-Kauwe, J. Xie, S. Hamm-Alvarez, Intracellular trafficking of nonviral vectors, Gene Ther. 12 (2005) 1734–1751.
[6] T. Gonen, Y. Cheng, P. Sliz, Y. Hiroaki, Y. Fujiyoshi, S.C. Harrison, T. Walz, Lipid–protein interactions in double-layered two-dimensional AQP0 crystals, Nature 438 (2005) 633–638.
[7] A.E. Regelin, S. Fankhaenel, L. Gurtesch, C. Prinz, G. von Kiedrowski, U. Massing, Biophysical and lipofection studies of DOTAP analogs, Biochim. Biophys. Acta 1464 (2000) 151–164.

[8] A.J. Lin, N.L. Slack, A. Ahmad, C.X. George, C.E. Samuel, C.R. Safinya, Biophys. J. 84 (2003) 3307–3316.
[9] F. Natali, C. Castellano, D. Pozzi, A.C. Castellano, Dynamic properties of an oriented lipid/DNA complex studied by neutron scattering, Biophys. J. 88 (2005) 1081–1090.
[10] S. Choosakoonkriang, C.M. Wiethoff, T. Anchordoquy, G.S. Koe, J.G. Smith, C.R. Maiddaugh, Infrared spectroscopic characterization of the interaction of cationic lipids with plasmid DNA, J. Biol. Chem. 276 (2001) 8037–8043.
[11] K. Schmidt-Rohr, J. Clauss, H.W. Spiess, Correlation of structure, mobility, and morphological information in heterogeneous polymer materials by two-dimensional wideline-separation NMR spectroscopy, Macromolecules 25 (1992) 3273–3277.
[12] R.K. Hester, J.L. Ackerman, B.L. Neff, J.S. Waugh, Separated local field spectra in NMR-determination of structure of solids, Phys. Rev. Lett. 36 (1976) 1081–1083.
[13] S.V. Dvinskikh, H. Zimmermann, A. Maliniak, D. Sandström, Measurements of motionally averaged heteronuclear dipolar couplings in MAS NMR using R-type recoupling, J. Magn. Reson. 168 (2004) 194–201.
[14] P.T. Callaghan, Principles of Nuclear Magnetic Resonance Microscopy, 1st ed.Oxford University Press, Oxford, 1991.
[15] W. Saenger, Principles of Nucleic Acid Structure, Springer Verlag, New York, 1984.
[16] C. Leal, L. Wadsö, G. Olofsson, M. Miguel, H. Wennerström, The hydration of a DNA–amphiphile complex, J. Phys. Chem., B 108 (2004) 3044–3050.
[17] M. Rosa, R. Dias, M. da Graça Miguel, B. Lindman, DNA-cationic surfactant interactions are different for double and single stranded DNA, Biomacromolecules 6 (2005) 2164–2171.
[18] A.E. Bennett, C.M. Rienstra, M. Auger, K.V. Lakshmi, R.G. Griffin, Heteronuclear decoupling in rotating solids, J. Chem. Phys. 103 (1995) 6951–6958.
[19] C. Leal, D. Topgaard, R.W. Martin, H. Wennerström, NMR studies of molecular mobility in a DNA–amphiphile complex, J. Phys. Chem., B 108 (2004) 15392–15397.
[20] X. Zhao, M. Edén, M.H. Levitt, Recoupling of heteronuclear dipolar interactions in solid-state NMR using symmetry-based pulse sequences, Chem. Phys. Lett. 342 (2001) 353–361.
[21] T. Nakai, T. Terao, Measurements of heteronuclear dipolar powder patterns due only to directly bonded couplings, Magn. Reson. Chem. 30 (1992) 42–44.
[22] S.V. Dvinskikh, V. Castro, D. Sandström, Efficient solid-state NMR methods for measuring heteronuclear dipolar couplings in unoriented lipid membrane systems, Phys. Chem. Chem. Phys. 7 (2005) 607–613.
[23] K. Wagner, D. Harries, S. May, V. Kahl, J.O. Radler, A. Ben-Shaul, Direct evidence for counterion release upon cationic lipid–DNA condensation, Langmuir 16 (2000) 303–306.
[24] J.O. Rädler, I. Koltover, T. Salditt, C.R. Safinya, Structure of DNA–cationic liposome complexes:DNA intercalation in multilamellar membranes in distinct interhelical packing regimes, Science 275 (1997) 810–814.
[25] T. Salditt, I. Koltover, J.O. Rädler, C.R. Safinya, Self-assembled DNA–cationic-lipid complexes: two-dimensional smectic ordering, correlations, and interactions, Phys. Rev., E Stat. Phys. Plasmas Fluids Relat. Interdiscip. Topics 58 (1998) 889–904.
[26] P.R. Cullis, B. Kruijff, Lipid polymorphism and the functional roles of lipids in biological membranes, Biochim. Biophys. Acta 559 (1979) 399–420.
[27] T. Terao, S. Matsui, K. Akasaka, 31P chemical shift anisotropy in solid nucleic acids, J. Am. Chem. Soc. 99 (1977) 6136–6138.
[28] J. Precechtelova, M.L. Munzarova, P. Novak, V. Sklenar, Relationships between 31P Chemical Shift Tensors and Conformation of Nucleic Acid Backbone: A DFT Study, J. Phys. Chem. B 111 (2007) 2658–2667.
[29] J.D. van Beek, matNMR: a flexible toolbox for processing, analyzing and visualizing magnetic resonance data in Matlab, J. Magn. Reson. 187 (2007) 19–26.
[30] J.W. Emsley (Ed.), Nuclear magnetic resonance of liquid crystals, D. Reidel Publishing Company, Dordrecht, 1985.
[31] S.J. Kohler, M.P. Klein, Orientation and dynamics of phospholipid head groups in bilayers and membranes determined from ’P nuclear magnetic resonance chemical shielding tensors? Biochemistry 16 (1977) 519–526.
[32] G. Lindblom, G. Gröbner, NMR on lipid membranes and their proteins, Curr. Opin. Colloid Interface Sci. 11 (2006) 24–29.
[33] G. Lindblom, G. Orädd, A. Filippov, Lipid lateral diffusion in bilayers with phosphatidylcholine, sphingomyelin and cholesterol. An NMR study of dynamics and lateral phase separation, Chem. Phys. Lipids 141 (2006) 179–184.
[34] I.V. Polozov, K. Gawrisch, Domains in binary SOPC/POPE lipid mixtures studied by pulsed field gradient H-1 MAS NMR, Biophys. J. 87 (2004) 1741–1751.
[35] S. Bandyopadhuay, M. Tarek, M.L. Klein, Molecular dynamics study of a lipid–DNA complex, J. Phys. Chem., B. 103 (1999) 10075–10080.
[36] R.S. Dias, A.A.C.C. Pais, P. Linse, M.G. Miguel, B. Lindman, Polyion adsorption onto catanionic surfaces. A Monte Carlo study, J. Phys. Chem., B 109 (2005) 11781–11788.
[37] B. Maier, J.O. Rädler, DNA on fluid membranes: a model polymer in two dimensions, Macromolecules 33 (2000) 7185–7194.
[38] W. Zhou, X. Weng, S. Jin, S. Rastogi, A.J. Lovinger, B. Lotz, S.Z.D. Cheng, Chain orientation and defects in lamellar single crystals of syndiotactic polypropylene fractions, Macromolecules 36 (2003) 9485–9491.
[39] D.C. Bassett, On Moiré patterns in electron microscopy of polymer crystals, Pill. Mag. 10 (1964) 595–615.
[40] D.B. Williams, C.B. Carter, Transmission Electron Microscopy: A textbook for Material Science, Plenum Press, New York, 1996.
[41] K. Schmidt-Rohr, H.W. Spiess, Multidimensional Solid-State NMR and Polymers, Academic Press, San Diego, 1994.
[42] M. Duer, Introduction to Solid-State NMR Spectroscopy, Blackwell Publishing Ltd, Oxford, 2004.
[43] J. Alper, R. Gelb, Standard errors and confidence intervals in nonlinear regression: comparison of Monte Carlo and parametric studies, J. Phys. Chem. 94 (1990) 4747–4751.
[44] F. Lindström, P. Williamson, G. Gröbner, Molecular insight into the electrostatic membrane surface potential by 14N/31P MAS NMR spectroscopy: nociceptin–lipid association, J. Am. Chem. Soc. 127 (2005) 6610–6616.
[45] J.H. Davis, The description of membrane lipid conformation, order and dynamics by ^{2}H-NMR, Biochim. Biophys. Acta 737 (1983) 117–171.
[46] J.D. Gross, D.E. Warschawski, R.G. Griffin, Dipolar recoupling in MAS NMR: a probe for segmental order in lipid bilayers, J. Am. Chem. Soc. 119 (1997) 796–802.
[47] H. Schiessel, H. Aranda-Espinoza, Electrostatically induced undulations of lamellar DNA–lipid complexes, Eur. Phys. J. E. 5 (2001) 499–506.
[48] D. Huster, U. Dietrich, T. Gutberlet, K. Gawrisch, K. Arnold, Lipid matrix properties in cationic membranes interacting with anionic polyelectrolytes: a solid-state NMR approach, Langmuir 16 (2000) 9225–9232.
[49] A. Salmon, S.W. Dodd, G.D. Williams, J.M. Beach, M.F. Brown, Configurational statistics of acyl chains in polyunsaturated lipid bilayers from deuterium NMR, J. Am. Chem. Soc. 109 (1987) 2600–2609.
[50] H. Schindler, J. Seelig, Deuterium order parameters in relation to thermodynamic properties of a phospholipid bilayer. A statistical mechanical interpretation, Biochemistry 14 (1975) 2283–2287.
[51] R.L. Thurmond, S.W. Dodd, M.F. Brown, Molecular areas of phospholipids as determined by 2H NMR spectroscopy, Biophys. J. 59 (1991) 108–113.
[52] J.F. Nagle, Area/lipid of bilayers from NMR, Biophys. J. 64 (1993) 1476–1481.
[53] J.E. Tanner, Use of stimulated echo in NMR diffusion studies, J. Chem. Phys. 52 (1970) 2523–2526.
[54] P.T. Callaghan, O. Söderman, Examination of the lamellar phase of aerosol OT/water using pulsed field gradient nuclear magnetic resonance, J. Phys. Chem. 87 (1983) 1737–1744.
[55] D. Topgaard, O. Söderman, Self-diffusion in two- and three-dimensional powders of anisotropic domains: an NMR study of the diffusion of water in cellulose and starch, J. Phys. Chem., B 106 (2002) 11887–11892.
[56] J.H. Davis, M. Auger, R.S. Hodges, High resolution 1H nuclear magnetic resonance of a transmembrane peptide, Biophys. J. 69 (1995) 1917–1932.

[57] H. Wennerström, Proton nuclear magnetic resonance lineshapes in lamellar liquid crystals, Chem. Phys. Lett. 18 (1973) 41–44.
[58] G. Rata, C. Leal, D. Topgaard, unpublished data.
[59] D.D. Lasic, H. Strey, M.C.A. Stuart, R. Podgornik, P.M. Frederik, The structure of DNA–liposome complexes, J. Am. Chem. Soc. 119 (1997) 832–833.
[60] K.P. Whittal, A.L. Mackay, Quantitative interpretation of NMR relaxation data, J. Magn. Reson. 84 (1989) 134–152.
[61] R.L. Parker, Y. Song, Assigning uncertainties in the inversion of NMR relaxation data, J. Magn. Reson. 174 (2005) 314–324.
[62] G. Lindblom, H. Wennerström, Amphiphile diffusion in model membrane systems studied by pulsed NMR, Biophys. Chemist. 6 (1977) 167–171.
[63] B. Balinov, U. Olsson, O. Söderman, Structural similarities between the L3 and bicontinuous cubic phases in the AOT-Brine system, J. Phys. Chem. 95 (1991) 5931–5936.